Electrostatic energy barriers from dielectric membranes upon approach of translocating DNA molecules

Sahin Buyukdagli, and T. Ala-Nissila

Citation: J. Chem. Phys. **144**, 084902 (2016); doi: 10.1063/1.4942177
View online: https://doi.org/10.1063/1.4942177
View Table of Contents: http://aip.scitation.org/toc/jcp/144/8
Published by the American Institute of Physics

Electrostatic energy barriers from dielectric membranes upon approach of translocating DNA molecules

Sahin Buyukdagli[1,a)] and T. Ala-Nissila[2,3,b)]
[1]*Department of Physics, Bilkent University, Ankara 06800, Turkey*
[2]*Department of Applied Physics and COMP Center of Excellence, Aalto University School of Science, P.O. Box 11000, Espoo, FI-00076 Aalto, Finland*
[3]*Department of Physics, Brown University, P.O. Box 1843, Providence, Rhode Island 02912-1843, USA*

(Received 17 November 2015; accepted 5 February 2016; published online 23 February 2016)

We probe the electrostatic cost associated with the approach phase of DNA translocation events. Within an analytical theory at the Debye-Hückel level, we calculate the electrostatic energy of a rigid DNA molecule interacting with a dielectric membrane. For carbon or silicon based low permittivity neutral membranes, the DNA molecule experiences a repulsive energy barrier between 10 k_BT and 100 k_BT. In the case of engineered membranes with high dielectric permittivities, the membrane surface attracts the DNA with an energy of the same magnitude. Both the repulsive and attractive interactions result from image-charge effects and their magnitude survive even for the thinnest graphene-based membranes of size $d \approx 6$ Å. For weakly charged membranes, the electrostatic energy is always attractive at large separation distances but switches to repulsive close to the membrane surface. We also characterise the polymer length dependence of the interaction energy. For specific values of the membrane charge density, low permittivity membranes repel short polymers but attract long polymers. Our results can be used to control the strong electrostatic energy of DNA-membrane interactions prior to translocation events by chemical engineering of the relevant system parameters. © *2016 AIP Publishing LLC.* [http://dx.doi.org/10.1063/1.4942177]

I. INTRODUCTION

The DNA molecule plays a crucial role in mediating biological information during the assembly of the building blocks of living organisms. As the carrier of the genetic code, DNA plays a central role in various biological and technological processes such as cell division,[1] protein biosynthesis,[2] drug delivery,[3] and DNA profiling.[4] The efficient use of DNA in biological and nanotechnological applications necessitates fast access to its genetic content and an accurate knowledge of its interaction with the surrounding medium. Considering the omnipresent coupling between strongly charged DNA molecules, the dielectric water solvent embodying charges, and external macromolecules and membranes in nature, a proper modelling of DNA electrostatics is essential.

A fundamental question concerning DNA in biological and artificial systems concerns the electrostatic interactions between fluctuating polymers and membranes. This has been mainly considered at the mean-field (MF) Poisson-Boltzmann (PB) level. The electrostatic MF approximation has the advantage of allowing the consideration of entropic polymer fluctuations. The corresponding formalism consists of coupling Edward's path integral model[5] with the field theoretic Coulomb liquid model.[6] In this context, one can mention the seminal works of Podgornik,[7,8] where he considered the electrostatics of an infinitely long polyelectrolyte between two charged membrane walls. Within the same MF approximation, the interaction of a polyelectrolyte with a charged sphere was considered in Ref. 9 and possible extensions beyond the MF level were proposed. Similar MF approaches have been subsequently applied to polyelectrolyte brushes[10] and polymer-interface interactions in incompressible liquids.[11]

Electrohydrodynamic theories of confined ions and polymers beyond the MF approximation have been developed for rigid polyelectrolytes. In Ref. 12, the present authors coupled one-loop electrostatic equations with the Stokes equation and calculated the electrophoretic DNA mobility and ionic currents in confined pores. Within this theory that accounts for charge correlations associated with low membrane permittivity and charge multivalency, we showed that the addition of multivalent counterions into the solution reverses the MF electrophoretic mobility of polyelectrolytes. It is noteworthy that this effect was recently observed in electrophoretic DNA transport experiments.[13] Then, by applying the theory to hydrodynamically induced DNA transport, we found that during polymer translocation events, the multivalency induced charge correlations reverse the ionic current through neutral pores.[14]

An important feature of the correlation-corrected polymer transport theories is that they neglect the interaction between the membrane and the portion of the DNA located outside the nanopore. In the present article, we address this issue by considering the electrostatic energy of a polyelectrolyte located in the vicinity a dielectric membrane. Our theory aims at quantitatively evaluating the electrostatic cost, i.e., the electrostatic contribution to the energy barrier, upon the approach phase preceding DNA translocation events. Understanding how to control this

a)Email: Buyukdagli@fen.bilkent.edu.tr
b)Email: Tapio.Ala-Nissila@aalto.fi

barrier is paramount to successful applications of DNA translocation.

At this point, we should also mention the important beyond-MF models of Refs. 15 and 16 where the effect of polarization charges on polymer adsorption onto planar interfaces was considered. The major approximation of these theories consists of replacing the electrostatic many-body potential by a one-body image-charge potential in the path integral over polymer configurations. In order to avoid the resulting uncontrollable errors and to simplify the theoretical framework, we consider here a rigid polyelectrolyte approaching a charged dielectric membrane. In the beginning of Section II, we calculate the electrostatic grand potential of the polymer induced by the presence of the membrane. Section II A is devoted to neutral membranes. We scrutinize the effect of the polymer length, salt density, and membrane thickness and permittivity on the grand potential of the polyelectrolyte. Then, in Section II B, we consider a charged membrane and investigate the competition between image charge and membrane surface charge forces in polymer-membrane interactions. The limitations and possible extensions of our theory are discussed in Sec. III.

II. DEBYE-HÜCKEL THEORY OF POLYMER-MEMBRANE INTERACTIONS

First, we introduce the theoretical model of electrostatic interactions between a DNA molecule and a dielectric membrane modelled as in Fig. 1. The membrane is assumed to consists of two infinite lateral surfaces on the $x-y$ plane, separated by d which is the membrane thickness. The left ($z<0$) and the right lateral surfaces ($z>d$) are in contact with a salt solution. The polyelectrolyte modelled as a rigid line charge of length L is located on the left side of the membrane. In Appendix A, we show that the electrostatic Debye-Hückel (DH) grand potential of the polyelectrolyte is

$$\Omega_{\rm pol}=k_BT\int\frac{\mathrm{d}\mathbf{r}\mathrm{d}\mathbf{r}'}{2}\sigma(\mathbf{r})v_{\rm DH}(\mathbf{r},\mathbf{r}')\sigma(\mathbf{r}'),\tag{1}$$

where $\sigma(\mathbf{r})$ is the distribution of the fixed charges (other than the mobile ions), and the Green's function $v_{\rm DH}(\mathbf{r},\mathbf{r}')$ is the solution of the DH Eq. (A8) introduced in Appendix A.

For the line charge perpendicular to the membrane, the total charge distribution can be expressed in the form

$$\sigma(\mathbf{r})=-\lambda\,\delta\left(\mathbf{r}_{\parallel}\right)\,g(z)+\sigma_s\delta(z),\tag{2}$$

where $\lambda>0$ is the linear DNA charge density, $\mathbf{r}_{\parallel}$ is the vector indicating the position of any point in the $x-y$ plane that coincides with the lateral membrane surface, and $g(z)$ stands for the polymer structure factor along the z axis. In the present work, we assume that the membrane surface charge of uniform density σ_s is located at $z=0$ and the second surface at $z=d$ is neutral. Furthermore, due to the translational symmetry in the membrane plane, one can Fourier expand the Green's function as

$$v_{\rm DH}(\mathbf{r},\mathbf{r}')=\int\frac{\mathrm{d}^2\mathbf{k}}{4\pi^2}\,e^{i\mathbf{k}\cdot\left(\mathbf{r}_{\parallel}-\mathbf{r}'_{\parallel}\right)}\tilde{v}_{\rm DH}(z,z').\tag{3}$$

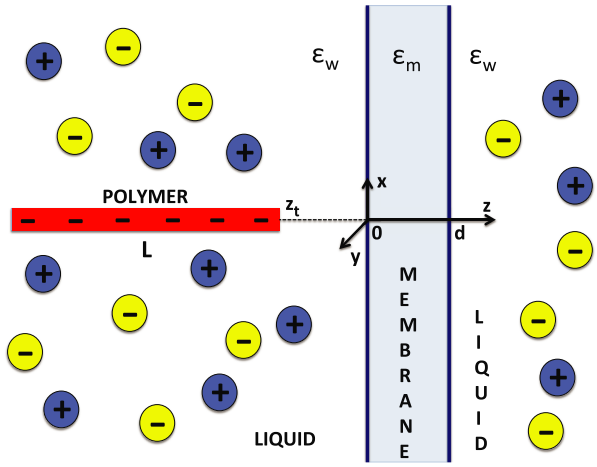

FIG. 1. Polyelectrolyte of length L and linear charge density $-\lambda<0$ whose right end is located at a distance of $z=z_t<0$ from the membrane. The membrane has thickness d and dielectric permittivity ε_m. Both the polymer and the membrane are immersed in a symmetric monovalent electrolyte solution with bulk concentration ρ_b and dielectric permittivity $\varepsilon_w=80$.

By inserting into the right-hand-side of Eq. (1) the function (2) together with the Fourier expansion (3) and evaluating the integrals over the membrane surface, the grand potential takes the form

$$\frac{\Omega_{\rm pol}}{k_BT}=\lambda^2\int_0^{\infty}\frac{\mathrm{d}kk}{4\pi}\iint_{-\infty}^{+\infty}\mathrm{d}z\mathrm{d}z'g(z)\tilde{v}_{\rm DH}(z,z')g(z')-\lambda\sigma_s\int_{-\infty}^{\infty}\mathrm{d}zg(z)\tilde{v}_{\rm DH}(z,z'=0;k=0).\tag{4}$$

In Eq. (4), we omitted the membrane self-energy $\Omega_{\rm mem}=\int_{\mathbf{r},\mathbf{r}'}\sigma_s(\mathbf{r})v_{\rm DH}(\mathbf{r},\mathbf{r}')\sigma_s(\mathbf{r}')/2$.

The quadratic dependence of the grand potential (4) on the polymer charge density λ is a result of the present DH approximation. This point is discussed in Appendix A in detail. The approximation is known to be valid at intermediate monovalent salt densities with $\rho_b\gtrsim 0.01$M. Although the nonlinear interactions neglected by the DH approach can be included by introducing a variational or one-loop level expansion of the grand potential,[24] this improvement will add to the numerical complexity and hide the analytical simplicity of our theory. This point is our main motivation for the choice of the present DH approximation. We finally note that in the rest of the article, we will consider a symmetric electrolyte composed of two monovalent species on each side of the membrane, with valencies $q_+=-q_-=1$ and bulk densities $\rho_{+b}=\rho_{-b}=\rho_b$. The liquid temperature will be set to the ambient temperature of $T=300$ K, and dielectric permittivities will be expressed in units of the vacuum permittivity ε_0.

A. Neutral membranes

Next, we will consider the interaction between the polyelectrolyte and a neutral membrane ($\sigma_s=0$). To this aim, we will calculate the net energetic cost for the polyelectrolyte to approach the membrane. In the configuration of the polymer of length L whose right end is located at the distance $z_t\leq 0$ from the membrane (see Fig. 1), the structure factor is given

by

$$g(z) = \theta(z_t - z)\theta(z - z_t + L), \tag{5}$$

where $\theta(x)$ is the Heaviside step function. We insert this structure factor into Eq. (4) together with the Fourier transformed Green's functions (B6)-(B8) given in Appendix B and subtract the electrostatic bulk grand potential associated with the bulk Green's function $\tilde{v}_b(z - z')$ of Eq. (B10). After carrying out the spatial integrals and noting that the second term of Eq. (4) vanishes for $\sigma_s = 0$, we get the net electrostatic grand potential mediated exclusively by the dielectric membrane in the form

$$\frac{\Delta\Omega_{\rm pol}(z_t)}{k_BT} = \frac{\ell_B\lambda^2}{2}\int_0^\infty \frac{{\rm d}kk}{p^3}\frac{\Delta\left(1-e^{-2kd}\right)}{1-\Delta^2e^{-2kd}} \times\left(1-e^{-pL}\right)^2e^{-2p|z_t|}. \tag{6}$$

The potential of Eq. (6) corresponds to the work done adiabatically to drive the polymer from the bulk region at $z = -\infty$ to the distance z_t from the membrane surface. In Eq. (6), we introduced the Bjerrum length $\ell_B = e^2/(4\pi\varepsilon_w k_BT) \approx 7$ Å with $\varepsilon_w = 80$ being the solvent permittivity, the auxiliary function $p = \sqrt{k^2+\kappa^2}$, where $\kappa^2 = 8\pi q^2\ell_B\rho_b$ stands for the DH screening parameter, and the dielectric discontinuity function $\Delta = (\varepsilon_w p - \varepsilon_m k)/(\varepsilon_w p + \varepsilon_m k)$. Moreover, the delta symbol on the l.h.s. of Eq. (6) means that we have neglected the bulk contribution and took into account exclusively the energy due to the presence of the membrane. Indeed, we note that in the limit of a bulk electrolyte, i.e., as the membrane thickness tends to zero $d \to 0$, the potential vanishes, that is, $\Delta\Omega_{\rm pol}(z_t) \to 0$ due to the membrane's neutrality assumption.

1. Membrane permittivity ε_m

The biological and synthetic membranes used in DNA translocation experiments are usually made of carbon or silicon. Such membranes are characterized by a low dielectric permittivity $\varepsilon_m \approx 2$–8. However, recent membrane engineering techniques based on the insertion of carbon structures or graphene nanoribbons (GNRs) into Si-based host matrices can increase the permittivity of these materials up to 8000.[17,18] In order to predict electrostatic membrane-polymer interactions over the experimentally relevant permittivity range, we plot in Fig. 2 the electrostatic grand potential of Eq. (6) for a polymer of length $L = 1$ μm against its distance z_t from the membrane for various permittivity values. The charge density is set to the linear charge density of dsDNA, that is, $\lambda = 2\,e/(0.34$ nm). The other model parameters are given in the figure caption.

In Fig. 2, for C/Si-based membranes with small permittivities ($\varepsilon_m = 2$), the grand potential of the approaching polymer increases from zero to about 11 k_BT within about 1 nm distance. The reduction of the barrier with increasing membrane permittivity (from top to bottom) shows that this energetic cost is mainly due to the interaction of the polymer charges with their electrostatic images. For the permittivity value $\varepsilon_m = \varepsilon_w = 80$, where the dielectric discontinuity between the liquid and the membrane vanishes, the barrier survives but its value is reduced by an order

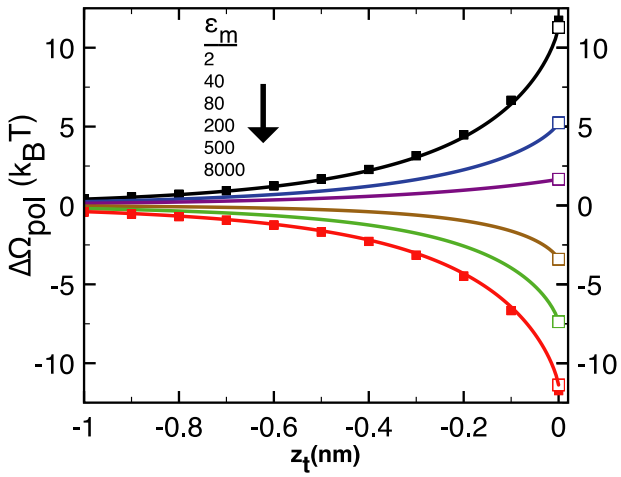

FIG. 2. The electrostatic grand potential of Eq. (6) against the polymer distance for various membrane permittivities displayed in the legend (solid curves). The bulk ion density is $\rho_b = 0.1$M, pore size $d = 10$ nm, polymer length $L = 1$ μm, and the DNA charge density $\lambda = 2\,e/(0.34$ nm). Open symbols denoting the energy barrier at $z_t = 0$ are from Eq. (8). Black and red symbols correspond to the closed-form expression of Eq. (14) with $\varepsilon_m = 0$ ($s = +1$) and $\varepsilon_m = \infty$ ($s = -1$), respectively.

of magnitude to $\Delta\Omega_{\rm pol}(0) \approx 2.0\ k_BT$. In the latter case where image-charge interactions are absent, the small barrier is solely due to the electrostatic screening deficiency of the charge-free membrane. More precisely, because the membrane is ion-free, the closer the polymer is to the membrane surface, the less efficient is the screening of its field by mobile ions. This effect translates into a solvation force oriented towards the bulk region where the electrostatic free energy of the polymer is lowest. Moreover, for GNRs type membranes with a large permittivity $\varepsilon_m > \varepsilon_w$, the electrostatic grand potential becomes *negative*. In other words, similar to point charges at metallic interfaces,[20] as the membrane dielectric permittivity exceeds that of water, the polymer-membrane interaction switches from repulsive to attractive. For the highest permittivity value $\varepsilon_m = 8000$ measured for GNRs,[17] the depth of the attractive well reaches a remarkably large value of $\Delta\Omega_{\rm pol}(0) \approx -11.0\ k_BT$.

We focus next on the electrostatic grand potential at $z_t = 0$. In order to derive an analytical expression, we consider the limit where the polymer length and the pore thickness tend to infinity, i.e., $L \to \infty$ and $d \to \infty$. The physical conditions that validate these limits will be determined below. In these limits, Eq. (6) simplifies to

$$\lim_{L,d\to\infty}\frac{\Delta\Omega_{\rm pol}(0)}{k_BT} = \frac{\ell_B\lambda^2}{2}\int_0^\infty\frac{{\rm d}kk}{p^3}\Delta. \tag{7}$$

Carrying out the integral and introducing the dielectric contrast parameter $\gamma = \varepsilon_m/\varepsilon_w$, the potential takes the form

$$\lim_{L,d\to\infty}\frac{\Delta\Omega_{\rm pol}(0)}{k_BT} = \frac{\ell_B\lambda^2}{2\kappa}F(\gamma), \tag{8}$$

with the auxiliary function

$$F(\gamma) = -1 + \frac{\pi}{\gamma} - \frac{2}{\gamma}\frac{\arccos(\gamma)}{\sqrt{1-\gamma^2}}, \quad \text{for} \quad \gamma < 1, \tag{9}$$

$$F(\gamma) = \pi - 3, \quad \text{for} \quad \gamma = 1, \tag{10}$$

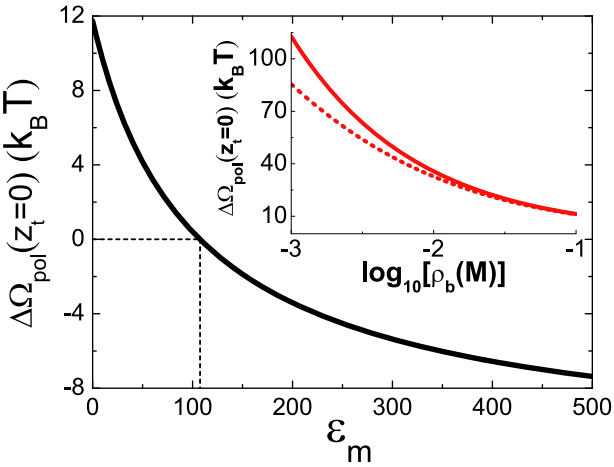

FIG. 3. The electrostatic grand potential of Eq. (8) at the membrane surface against membrane permittivity ε_m at density $\rho_b = 0.1$M (main plot) and salt concentration ρ_b at permittivity $\varepsilon_m = 2$ (solid curve in the inset). The dashed curve in the inset obtained from Eq. (6) for $L \to \infty$, $\varepsilon_m = 2$, and $d = 6$ Å generalizes the result in the solid curve to a finite membrane thickness. The remaining model parameters are the same as in Fig. 2.

$$F(\gamma) = -1 + \frac{\pi}{\gamma} - \frac{2}{\gamma}\frac{\ln\left[\gamma + \sqrt{\gamma^2 - 1}\right]}{\sqrt{\gamma^2 - 1}}, \quad \text{for} \quad \gamma > 1. \tag{11}$$

In Fig. 2, we show that the simple law of Eq. (8) accurately reproduces the electrostatic grand potential at $z_t = 0$ for various membrane permittivities (open square symbols at zero distance).

In the main plot of Fig. 3, we show the potential of Eq. (8) on the membrane surface versus the membrane permittivity. In agreement with Fig. 2, with an increase of the permittivity from $\varepsilon_m = 2$ to 500, the potential is seen to change from $+12\ k_BT$ to $-8\ k_BT$. As indicated by the dashed lines in the same figure, it switches from repulsive to attractive at the permittivity value $\varepsilon_m \approx 107$, where the weak attractive image force exactly compensates for the repulsive solvation force induced by the charge screening deficiency of the membrane. In Subsection II A 2, we scrutinize the polymer length and salt dependence of this interaction energy.

2. Polymer length L and salt density ρ_b

DNA translocation experiments are carried out with different sequence lengths and salt concentrations. Motivated by this, we focus next on the salt and polymer length dependence of the DNA-membrane interactions. To this aim, we will derive a closed-form expression for the electrostatic grand potential profile of Eq. (6) in the case of very low and very large permittivity membranes. First, we introduce an auxiliary parameter s that will allow to cover the case of biological or silicon-based membranes of low permittivities ($\varepsilon_m \ll \varepsilon_w$) and engineered membranes including GNRs of large permittivities ($\varepsilon_m \gg \varepsilon_w$),[18]

$$s = +1, \quad \text{for} \quad \varepsilon_m = 0 \ \text{(bio/Si membranes)}, \tag{12}$$

$$s = -1, \quad \text{for} \quad \varepsilon_m = \infty \ \text{(GNRs)}. \tag{13}$$

In the upper and lower limits defined by Eqs. (12) and (13), the dielectric discontinuity function Δ in Eq. (6) tends to $+1$ and -1, respectively, which allows to carry out the Fourier integral. We find

$$\Delta\Omega_{\rm pol}(z_t) = sk_BT\frac{\ell_B\lambda^2}{2\kappa}G(z_t), \tag{14}$$

where we defined the adimensional function

$$\begin{aligned} G(z_t) = {} & e^{2\kappa z_t} + e^{-2\kappa(L-z_t)} - 2e^{-\kappa(L-2z_t)} \\ & - 2\kappa z_t\ \mathrm{Ei}[2\kappa z_t] + 2\kappa(L-z_t)\mathrm{Ei}\left[-2\kappa(L-z_t)\right] \\ & - 2\kappa(L-2z_t)\mathrm{Ei}\left[-\kappa(L-2z_t)\right]. \end{aligned} \tag{15}$$

In Eq. (15), the exponential integral function is denoted by $\mathrm{Ei}(x)$.[19] We display the grand potential of Eq. (14) in Fig. 2 by solid square symbols. We note that this analytical form accurately reproduces the energy profile for low permittivity ($\varepsilon_m = 2$) and large permittivity ($\varepsilon_m = 8000$) membranes. Using the closed-form expression of Eq. (14), we will next scrutinize the dependence of the electrostatic grand potential on the polymer length and ion concentration.

In Fig. 4, we display the polymer length dependence of the electrostatic grand potential Eq. (14) on the membrane surface

$$\frac{\Delta\Omega_{\rm pol}(0)}{s\Delta\Omega^*} = \left(1 - e^{-\kappa L}\right)^2 + 2\kappa L\left[\mathrm{Ei}(-2\kappa L) - \mathrm{Ei}(-\kappa L)\right], \tag{16}$$

for $\varepsilon_m = 0$ ($s = +1$), where we have rescaled the electrostatic grand potential by the characteristic energy

$$\Delta\Omega^* = k_BT\frac{\ell_B\lambda^2}{2\kappa}. \tag{17}$$

We can see that the potential given by Eq. (16) increases steadily with the polymer length up to $L \approx \kappa^{-1}$ and converges towards the saturation value $\lim_{L,d\to\infty}\Delta\Omega_{\rm pol}(0) = s\Delta\Omega^*$ beyond which it does not depend on the polymer length. The relation of Eq. (17) shows that for long polymers $\kappa L \gg 1$, the electrostatic grand potential on the membrane surface scales with ion density as $\Delta\Omega_{\rm pol}(0) \propto \rho_b^{-1/2}$.

In order to get further analytical insight into the length dependence of the grand potential at the membrane surface, we Taylor expand Eq. (16). We find that for dilute electrolytes or

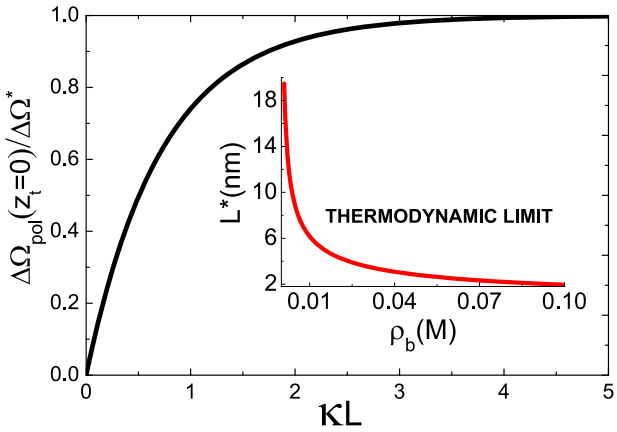

FIG. 4. Main plot: The rescaled electrostatic grand potential of Eq. (16) at the membrane surface against the reduced polymer length κL at the membrane permittivity $\varepsilon_m = 0.0$. Inset: The characteristic polymer length $L^* = 2/\kappa$ above which the thermodynamic limit is reached (area above the curve) against the bulk salt density.

short polymers $\kappa L \ll 1$, the grand potential increases linearly with length,

$$\Delta\Omega_{\rm pol}(0) = s\ln(2)k_BT\lambda^2\ell_B L + O\left[(\kappa L)^2\right]. \quad (18)$$

At large lengths or in strong salt solutions $\kappa L \gg 1$, the potential reaches exponentially fast the strict thermodynamic limit of Eq. (17),

$$\Delta\Omega_{\rm pol}(0) = sk_BT\frac{\ell_B\lambda^2}{2\kappa}\left\{1+\frac{2}{\kappa L}\left(\frac{2}{\kappa L}-1\right)e^{-\kappa L}\right\} + O\left(e^{-2\kappa L}\right). \quad (19)$$

Moreover, defining the saturation condition of the grand potential as $\Delta\Omega_{\rm pol}(z_t = 0) \gtrsim 0.9\Delta\Omega^*$, we find that the former saturates at $\kappa L \gtrsim 2$. This yields the characteristic polymer length determining the thermodynamic limit as $L^* = 2/\kappa$. We plot the latter equality in the inset of Fig. 4. We see that the higher the salt concentration, the smaller the thermodynamic length. Indeed, we find $L^* \approx 20$ nm (equivalent to ≈100 bps dsDNA sequences) at the salt density $\rho_b = 10^{-3}$M, $L^* \approx 6$ nm (≈30 bps) for $\rho_b = 10^{-2}$M, and $L^* \approx 2$ nm (≈10 bps) at $\rho_b = 10^{-1}$M. It is noteworthy that beyond these critical lengths where finite size effects are irrelevant, the electrostatic grand potential of Eq. (14) takes for $L \to \infty$ a much simpler form

$$\Delta\Omega_{\rm pol}(z_t) = sk_BT\frac{\ell_B\lambda^2}{2\kappa}\left[e^{-2\kappa|z_t|} + 2\kappa|z_t|\,{\rm Ei}(-2\kappa|z_t|)\right]. \quad (20)$$

After having investigated the short distance behaviour of the electrostatic grand potential, we now consider its large distance behaviour. By Taylor-expanding Eq. (14) in the regime $|\kappa z_t| \gg 1$, we find to leading order

$$\Delta\Omega_{\rm pol}(z_t) \approx sk_BT\frac{\ell_B Q_{\rm eff}^2(L)}{4|z_t|}e^{-2\kappa|z_t|}. \quad (21)$$

In Eq. (21), we have introduced the effective polymer charge

$$Q_{\rm eff}(L) = \lambda L\,\frac{1-e^{-\kappa L}}{\kappa L}. \quad (22)$$

Interestingly, Eq. (21) has exactly the form of the image-charge potential experienced by a point ion of valency $Q_{\rm eff}(L)$ located at the distance $-z_t$ from a dielectric interface.[20] Equations (21) and (22) indicate that in dilute salt solutions or for short sequence lengths, polymers far away from the membrane interact with the latter as point charges with valency $Q_{\rm eff}(L \ll \kappa^{-1}) = L\lambda$. Thus, in this physical regime, polymer-membrane interactions are governed by the bare polymer charge. In the opposite case of long DNA sequences or strong salt, the effective charge takes the form $Q_{\rm eff}(L \gg \kappa^{-1}) = \lambda/\kappa$, indicating that the intensity of the interactions is set by the net charge of the polymer dressed by the surrounding counterion cloud.

Since the salt concentration is an easily controllable parameter in translocation experiments, it is important to characterize the influence of salt on the range and the magnitude of the polymer's grand potential. In the inset of Fig. 3 where we plot Eq. (8) (solid red curve), we see that the lower the salt concentration, the larger the electrostatic grand potential at the membrane surface. More precisely, the reduction of the ion density from $\rho_b = 10^{-1}$M to 10^{-3}M increases the grand potential by an order of magnitude from ≈10 k_BT to ≈100 k_BT. In order to consider the range of the interactions, we remove finite size effects and focus on the limit $L \to \infty$. By Taylor expanding Eq. (20) for large distances $|\kappa z_t| \gg 1$, we get the electrostatic grand potential in the asymptotic form

$$\Delta\Omega_{\rm pol}(z_t) \approx sk_BT\frac{\ell_B\lambda^2}{4\kappa^2|z_t|}e^{-2\kappa|z_t|} = s\Delta\Omega^*\frac{e^{-2\kappa|z_t|}}{2\kappa|z_t|}. \quad (23)$$

In the second equality of Eq. (23), we have separated the surface energy barrier of Eq. (17) and the Yukawa type of decay function $e^{-2\kappa|z_t|}/2\kappa|z_t|$. Numerically, we find that this function reduces the energy by an order of magnitude at the distance $2\kappa|z_t| \approx 2$, which fixes the characteristic range of the interaction as $z^* = \kappa^{-1}$. This equality yields $z^* \approx 1.0$ nm for $\rho_b = 10^{-1}$M (see also Fig. 2), $z^* \approx 3.0$ nm at $\rho_b = 10^{-2}$M, and $z^* \approx 10$ nm at $\rho_b = 10^{-3}$M. Therefore, the reduction of the salt density significantly increases the range of polymer-membrane interactions.

Before concluding, we consider the range of polymer-membrane interactions in a pure solvent. Neglecting the screening parameter κ, taking the large pore limit $d \to \infty$, and introducing the reduced separation distance $\bar{z}_t = |z_t|/L$, we can carry out the integral of Eq. (14) and get

$$\Delta\Omega_{\rm pol}(z_t) = k_BT\ell_B L\lambda^2\Delta_0\left\{\ln\left[\frac{2+2\bar{z}_t}{1+2\bar{z}_t}\right] - \bar{z}_t\ln\left[\frac{(1+2\bar{z}_t)^2}{4\bar{z}_t(\bar{z}_t+1)}\right]\right\}, \quad (24)$$

with the salt-free dielectric discontinuity parameter $\Delta_0 = (\varepsilon_w - \varepsilon_m)/(\varepsilon_w + \varepsilon_m)$. We now note that at large separation distances $|z_t| \gg L$, the grand potential of Eq. (24) decays algebraically as

$$\Delta\Omega_{\rm pol}(z_t) \approx k_BT\Delta_0\frac{\ell_B(\lambda L)^2}{4|z_t|}. \quad (25)$$

Equation (25) has the form of the electrostatic image potential of a point charge with valency $Q_{\rm eff} = \lambda L$ located at a distance $|z_t|$ from a dielectric interface.[20] The form of this grand potential indicates that in pure solvents or dilute electrolytes with $\kappa L \ll 1$, the range of polymer-membrane interactions is set by the Bjerrum length ℓ_B. In other words, the charge screening is replaced by the dielectric screening. Next, we investigate the effect of the membrane thickness on the strength of these interactions.

3. Membrane thickness d

Artificial membranes used in translocation experiments possess various thicknesses ranging from $d = 6$ Å for graphene-based membranes[21] to $d = 250$ nm for Si-based membranes.[22] Motivated by this fact, we investigate next the influence of the membrane thickness d on the electrostatic grand potential. We first consider the salt-free limit $\rho_b \to 0$ of pure solvents. To this end, we set in Eq. (6) $z_t = 0$ and $\kappa = 0$. Introducing again the salt-free dielectric discontinuity parameter $\Delta_0 = (\varepsilon_w - \varepsilon_m)/(\varepsilon_w + \varepsilon_m)$ and the new integration variable $q = kL$, the grand potential of Eq. (6) becomes

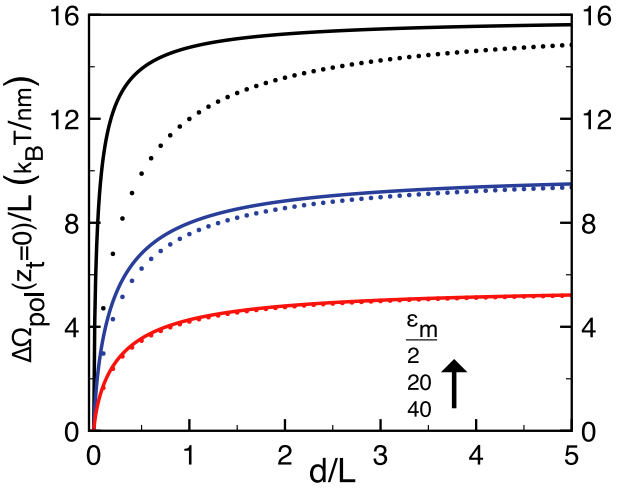

FIG. 5. The electrostatic grand potential per polymer length Eq. (26) at the membrane surface versus the ratio d/L in pure solvents ($\rho_b = 0$) for various membrane permittivities displayed in the legend (solid curves). Dotted curves display the closed-form expression of Eq. (28). The model parameters are the same as in Fig. 2.

$$\frac{\Delta\Omega_{\rm pol}(0)}{k_BTL} = \frac{\Delta_0\ell_B\lambda^2}{2}\int_0^\infty \frac{dq}{q^2}\frac{\left(1-e^{-2qd/L}\right)}{1-\Delta_0^2e^{-2qd/L}}\times\left(1-e^{-q}\right)^2. \tag{26}$$

The integral term of Eq. (26) accounting for finite size effects depends solely on the ratio d/L. This indicates that finite size effects are governed by competition between the pore thickness and the polymer length. We plot the electrostatic grand potential per length in Eq. (26) in Fig. 5. Due to the strengthening of the image interactions, the amplitude of the potential on the membrane surface increases with the membrane thickness d from zero to the saturation value

$$\lim_{d\to\infty}\Delta\Omega_{\rm pol}(0) \approx \Delta_0 k_BT\ell_BL\lambda^2\ln(2). \tag{27}$$

In order to explain the non-linear shape of the grand potential curves in Fig. 5, one can derive an approximate closed-form expression. To this end, we carry out the integral in Eq. (26) by neglecting the function in the denominator, which consists of considering the first dielectric images only. Introducing the adimensional pore size $\bar{d} = d/L$ to simplify the notation gives

$$\frac{\Delta\Omega_{\rm pol}(0)}{k_BTL} \approx \frac{\Delta_0\ell_B\lambda^2}{2}\left\{\ln\left[\frac{1+2\bar{d}}{1+\bar{d}}\right] + \bar{d}\ln\left[\frac{(1+2\bar{d})^2}{4\bar{d}(1+\bar{d})}\right]\right\}. \tag{28}$$

In Fig. 5, we show that this analytic formula reproduces the result of the integral relation of Eq. (26) with quantitative accuracy for moderate dielectric discontinuities and qualitatively for strong dielectric jumps. According to Eq. (28), for membranes with thicknesses much smaller than the polymer length $d \ll L$, the electrostatic grand potential grows linearly with the ratio d/L as

$$\Delta\Omega_{\rm pol}(0) \approx \Delta_0 k_BT\ell_BL\lambda^2\left\{1-\ln\left(\frac{4d}{L}\right)\right\}\frac{d}{L}, \tag{29}$$

while for thick membranes $d \gg L$, the grand potential converges towards the asymptotic value of Eq. (27) according to the inverse algebraic relation

$$\Delta\Omega_{\rm pol}(0) \approx \Delta_0 k_BT\ell_BL\lambda^2\left\{\ln(2) - \frac{L}{4d}\right\}. \tag{30}$$

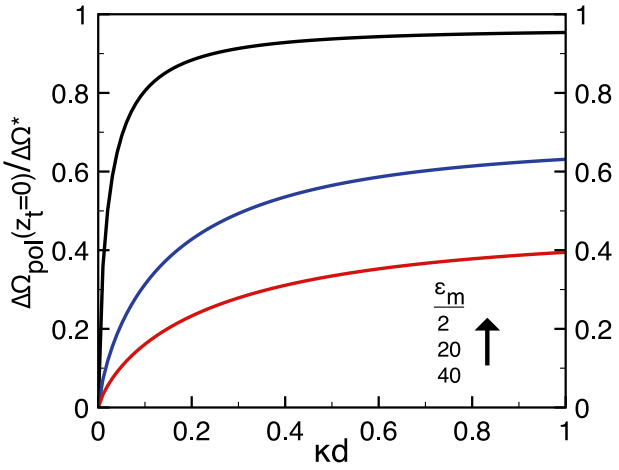

FIG. 6. The electrostatic grand potential of Eq. (31) at the membrane surface rescaled by the characteristic energy $\Delta\Omega^*$ of Eq. (17) versus the ratio κd for different membrane permittivities displayed in the legend. The model parameters are the same as in Fig. 2.

Figure 5 indicates that the saturation sets in between these two regimes at $d \approx L$. Thus, in pure solvents, finite pore size effects are negligible as long as the pore thickness is larger than the polymer length.

We investigate next the effect of the membrane thickness on membrane-polymer interactions at finite salt density. In order to simplify the analysis, we consider the thermodynamic limit $\kappa L \to \infty$ scrutinized in Section II A 2 and sketched in Fig. 4. Introducing the adimensional wave vector $q = k/\kappa$ and setting $z_t = 0$, the electrostatic grand potential of Eq. (6) rescaled with Eq. (17) becomes

$$\frac{\Delta\Omega_{\rm pol}(0)}{\Delta\Omega^*} = \int_0^\infty \frac{dqq}{\bar{p}^3}\frac{\bar{\Delta}\left(1-e^{-2q\kappa d}\right)}{1-\bar{\Delta}^2e^{-2q\kappa d}}, \tag{31}$$

where we introduced the adimensional parameters $\bar{p} = \sqrt{1+q^2}$ and $\bar{\Delta} = (\bar{p}-\gamma q)/(\bar{p}+\gamma q)$. In Fig. 6, the plot of Eq. (31) shows that the increase of the adimensional thickness κd is accompanied by the rise of the electrostatic grand potential towards the upper boundary determined by Eq. (8). Thus, the lower the salt density, the more pronounced the finite membrane size effects. Moreover, at given salt density, the stronger the dielectric contrast, the smaller the characteristic membrane thickness where the potential saturates.

In order to quantitatively determine the physical conditions where finite membrane size matters, we calculate with Eq. (31) the characteristic membrane size d^* where the electrostatic grand potential saturates. We find that at the permittivity $\varepsilon_m = 2$ of carbon-based membranes, the saturation of the function $\Delta\Omega_{\rm pol}(0)/\Delta\Omega^*$ occurs at $\kappa d^* \approx 0.165$. This yields $d^* \approx 2$ Å at the salt density $\rho_b = 0.1$M, $d^* \approx 5$ Å for $\rho_b = 0.01$M, and $d^* \approx 1.6$ nm at $\rho_b = 0.001$M. These values indicate that in DNA translocation experiments, even the thinnest graphene-based membranes of thickness $d = 6$ Å[21] can be considered in the thermodynamic regime $\kappa d \to \infty$ as long as the salt density is above the value

$\rho_b \approx 0.01$M. This is shown in the inset of Fig. 3 where we compare the electrostatic grand potential at the surface of a membrane with finite thickness $d = 6$ Å (dashed curve) and in the limit $d \to \infty$ (solid curve). One sees that finite size effects become indeed noticeable for $\rho_b \lesssim 0.01$M but the electrostatic energy barrier $\Delta\Omega_{\rm pol}(0) \approx 80\ k_BT$ still remains very large in this density regime. This shows that polymer-membrane interactions induced by dielectric images are relevant even for sub-nanometer membrane thicknesses.

B. Charged membranes

Depending on the pH of the solution, membrane surfaces subject to protonation processes may possess a finite average charge distribution. Motivated by this fact, we consider next the coupling between the polymer and the membrane charge. This is taken into account by the second term of Eq. (4). As we found that finite membrane size corrections are irrelevant in physiological conditions, we take the infinitely thick membrane limit $d \to \infty$. Inserting the structure factor of Eq. (5) into Eq. (4) together with Fourier-transformed Green's functions (B6)-(B8), we get after some algebra the electrostatic grand potential in the form

$$\frac{\Delta\Omega_{\rm pol}(z_t)}{k_BT} = \frac{\ell_B\lambda^2}{2}\int_0^\infty \frac{{\rm d}k\,k}{p^3}\Delta\left(1-e^{-pL}\right)^2 e^{-2p|z_t|} - \frac{2Q_{\rm eff}(L)}{\mu\kappa}\,e^{-\kappa|z_t|}. \tag{32}$$

In Eq. (32), we introduced the Gouy-Chapman length $\mu^{-1} = 2\pi\ell_B\sigma_s$ and used the effective polyelectrolyte charge $Q_{\rm eff}(L)$ of Eq. (22).

1. Membrane charge σ_s

In order to understand the influence of the membrane charge on the polymer's grand potential, we focus on the most relevant case of very low and very large permittivity membranes (see Eqs. (12) and (13)). Within this restriction, the grand potential of Eq. (32) takes the form

$$\frac{\Delta\Omega_{\rm pol}(z_t)}{k_BT} = s\frac{\ell_B\lambda^2}{2\kappa}G(z_t) - \frac{2Q_{\rm eff}(L)}{\mu\kappa}\,e^{-\kappa|z_t|}, \tag{33}$$

with the function $G(z_t)$ introduced in Eq. (15). We consider a positively charged membrane $\sigma_s \geq 0$ of low permittivity $\varepsilon_m \ll \varepsilon_w$ and set $s = +1$. In Fig. 7, we plot the potential profile of Eq. (33) at salt density $\rho_b = 0.01$M for various membrane charges up to $\sigma_s = 0.1\ e/{\rm nm}^2$. Due to the attractive term on the r.h.s. of Eq. (33), increasing membrane charge results in lowering of the grand potential which eventually switches from positive to negative. More precisely, it acquires a negative branch associated with a minimum located at $z_t \approx -1$ nm. We see that for the largest value $\sigma_s = 0.1\ e/{\rm nm}^2$ which still corresponds to a weakly charged membrane, the depth of the energy well is significantly large at about $-25\ k_BT$. In translocation experiments, the presence of such a deep well may allow to control the approach velocity of DNA by tuning the chemical properties of the membrane surface.

Next, we focus on the large distance behaviour $\kappa z_t \gg 1$ of the electrostatic grand potential of Eq. (33). To leading order, the latter takes the form

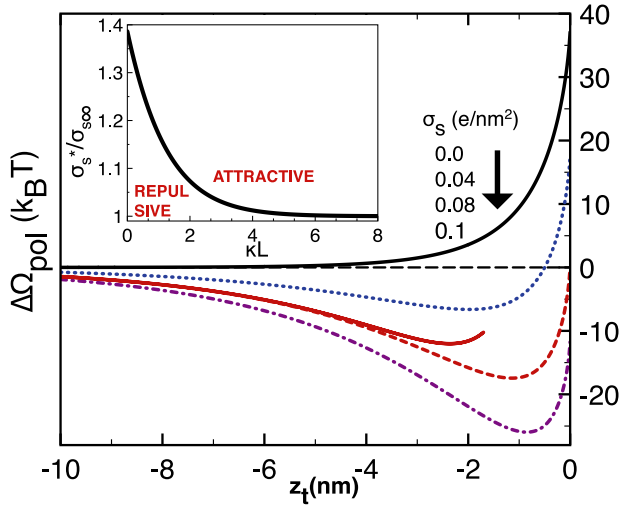

FIG. 7. Main plot: The electrostatic grand potential profile (Eq. (33)) at membrane permittivity $\varepsilon_m = 0$, polymer length $L = 1.0$ μm, salt density $\rho_b = 10^{-2}$M, and various surface charges as displayed in the legend. The solid red curve is from the asymptotic large distance law of Eq. (34). Inset: Characteristic surface charge (Eq. (36)) separating the attractive and repulsive membrane regimes rescaled by the long polymer limit of Eq. (38) against the adimensional polymer length κL. The remaining model parameters are the same as in Fig. 2.

$$\frac{\Delta\Omega_{\rm pol}(z_t)}{k_BT} = \frac{\ell_BQ_{\rm eff}^2(L)}{4|z_t|}e^{-2\kappa|z_t|} - \frac{2Q_{\rm eff}(L)}{\kappa\mu}e^{-\kappa|z_t|}. \tag{34}$$

This has exactly the form of the net electrostatic potential of a point charge $Q_{\rm eff}(L)$ located at distance z_t from a charged dielectric wall.[20] The functional form of Eq. (34) plotted in Fig. 7 (solid red curve) explains the negative sign of the polymer's grand potential far away from the surface: the polymer-surface charge attraction (the second term), being longer ranged than the image charge repulsion (the first term), dominates the repulsive image interactions at large separation distances. This means that in the presence of a finite surface charge, the polymer's grand potential will always have an attractive branch far enough from the interface.

2. Polymer length L and salt density ρ_b

In order to consider the influence of the polymer length on the electrostatic grand potential of the DNA close to a charged membrane, we investigate the short distance behaviour of polymer-membrane interactions. The form of the grand potential at the membrane surface for the permittivity $\varepsilon_m = 0$,

$$\frac{\Delta\Omega_{\rm pol}(0)}{k_BT} = \frac{\ell_B\lambda^2}{2\kappa}G(0) - \frac{2Q_{\rm eff}(L)}{\kappa\mu}, \tag{35}$$

suggests that there exists a characteristic membrane charge σ_s^* where the potential on the surface vanishes. In Fig. 7, this corresponds to the dashed red curve at $\sigma_s = 0.08\ e/{\rm nm}^2$. By equating Eq. (35) to zero and inverting the relation, the critical charge can be expressed as

$$\sigma_s^* = \frac{\kappa\lambda}{8\pi}\frac{\left(1-e^{-\kappa L}\right)^2 + 2\kappa L\left[{\rm Ei}(-2\kappa L) - {\rm Ei}(-\kappa L)\right]}{1-e^{-\kappa L}}. \tag{36}$$

We plot Eq. (36) in the inset of Fig. 7. Increasing the reduced polymer length κL, the critical charge drops smoothly from

$$\sigma_{s0} \approx 2\ln(2)\frac{\kappa\lambda}{8\pi}, \tag{37}$$

for $\kappa L \ll 1$ to

$$\sigma_{s\infty} \approx \frac{\kappa\lambda}{8\pi}, \tag{38}$$

for $\kappa L \gg 1$. We note that in both limits the characteristic charge is independent of the polymer length.

We consider next the length dependence of the electrostatic grand potential of Eq. (35). For short polymers $\kappa L \ll 1$, it takes the asymptotic form

$$\frac{\Delta\Omega_{\rm pol}(0)}{\Delta\Omega^*} \approx 2\ln(2)\left[1-\frac{\sigma_s}{\sigma_{s0}}\right]\kappa L \tag{39}$$

which switches from repulsive to attractive at $\sigma_s = \sigma_{s0}$. For long polymers $\kappa L \gg 1$, the grand potential reads

$$\frac{\Delta\Omega_{\rm pol}(0)}{\Delta\Omega^*} \approx 1-\frac{\sigma_s}{\sigma_{s\infty}} \tag{40}$$

which turns from positive to negative at $\sigma_s = \sigma_{s\infty}$. This is illustrated in Fig. 8(a), where we plot Eq. (35) versus κL. Reducing the membrane charge from $\sigma_s = \sigma_{s\infty}/2$ to $\sigma_s = \sigma_{s\infty}$, the long polymer limit drops to zero while the electrostatic grand potential remains repulsive ($\Delta\Omega_{\rm pol}(0) > 0$) for short polymers $L \approx \kappa^{-1}$. At the larger charge value $\sigma_s = 1.07\sigma_{s\infty}$, the grand potential at the membrane surface is repulsive for short polymers, but attractive ($\Delta\Omega_{\rm pol}(0) < 0$) for long polymers. Increasing the membrane charge to $\sigma_s = \sigma_{s0} > \sigma_{s\infty}$, in agreement with Eq. (40), polymer-membrane interactions become attractive for all polymer lengths.

In Fig. 8(b), we also consider the influence of salt. The increase of the salt density switches the polymer-membrane interaction from attractive to repulsive. Indeed, inverting the limiting laws of Eqs. (37) and (38), we find that the critical screening parameter where the grand potential on the surface switches from negative to positive is $\kappa_0 = 8\pi\sigma_s/[2\ln(2)\lambda]$ for short polymers ($\kappa L \ll 1$) and $\kappa_\infty = 8\pi\sigma_s/\lambda$ for long polymers ($\kappa L \gg 1$). Thus, salt weakens the relative weight of the attractive surface charge effect with respect to repulsive image-charge interactions.

3. Membrane permittivity ε_m

Finally, we scrutinize the influence of the membrane permittivity. Taking the limit $d \to \infty$ and $L \to \infty$, Eq. (34) yields the electrostatic grand potential at the membrane surface in an analytic form as

$$\frac{\Delta\Omega_{\rm pol}(0)}{k_BT} = \frac{\ell_B\lambda^2}{2\kappa}F(\gamma) - \frac{2\lambda}{\kappa^2\mu}, \tag{41}$$

with the parameter $\gamma = \varepsilon_m/\varepsilon_w$ and the function $F(\gamma)$ given by Eqs. (9)-(11). In Fig. 9, we plot the potential of Eq. (41) against the bulk ion density for various membrane permittivities. For a typical permittivity value of $\varepsilon_m = 2$ for carbon-based membranes, where polymer-membrane interactions are governed by repulsive image forces (the first term of Eq. (41)), the positive grand potential drops monotonically with ion density. At the intermediate value $\varepsilon_m = 40$ where image forces weaken, the electrostatic grand potential remains positive but exhibits a peak at the density $\rho_b \approx 3\times10^{-3}$M, below which the energetic cost decreases. This corresponds to the physical regime where the membrane charge attraction becomes relevant. By taking the derivative of Eq. (41) with respect to the screening parameter, we find that the peak is located at the bulk concentration

$$\rho_{b,c} = \frac{32\pi\sigma_s^2}{\ell_B\lambda^2F^2(\gamma)}. \tag{42}$$

We note that for $\varepsilon_m < 107$ (i.e., $F(\gamma) > 0$) and $\sigma_s > 0$, this density associated with the maximum energetic barrier increases both with the membrane charge ($\sigma_s \uparrow \rho_{b,c} \uparrow$) and the membrane permittivity ($\varepsilon_m \uparrow \rho_{b,c} \uparrow$). Then, at the

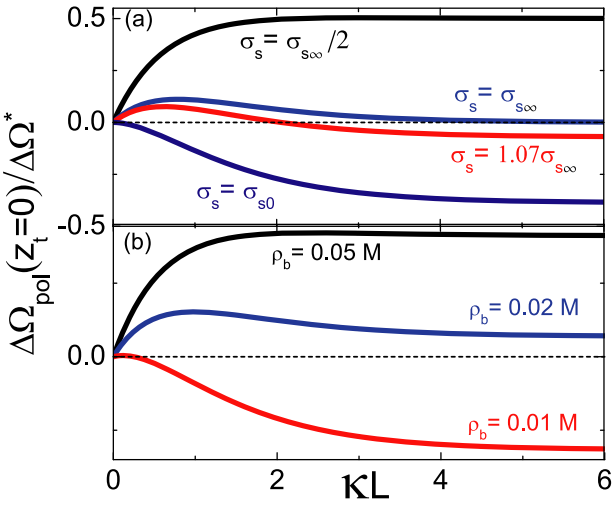

FIG. 8. The electrostatic grand potential of Eq. (35) on the membrane surface rescaled by the characteristic energy $\Delta\Omega^*$ of Eq. (17) versus the adimensional polymer length κL for various (a) surface charges and (b) salt densities at the permittivity $\varepsilon_m = 0$. In (a), the salt density is $\rho_b = 0.01$M and in (b), the surface charge is $\sigma_s = 0.1\ e/\text{nm}^2$.

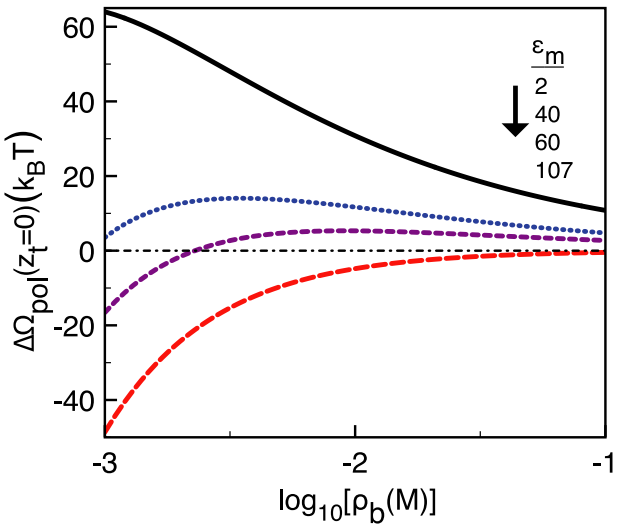

FIG. 9. The electrostatic grand potential at the membrane surface (Eq. (41)) versus the bulk electrolyte density ρ_b at the membrane charge $\sigma_s = 0.01\ e/\text{nm}^2$ for various membrane permittivities given in the legend. The remaining model parameters are the same as in Fig. 2.

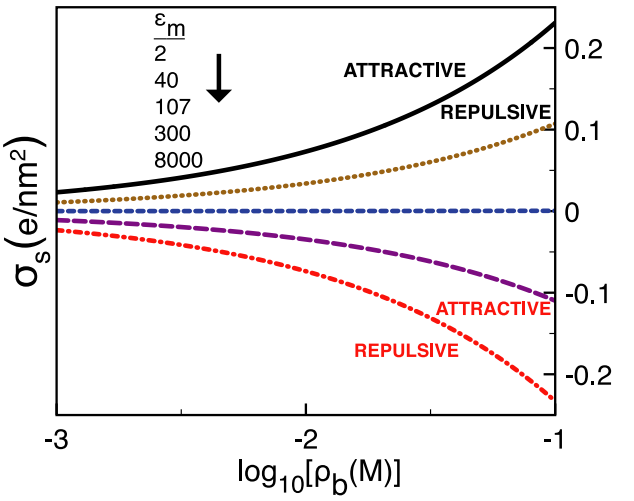

FIG. 10. Phase diagram: the membrane charge (Eq. (43)) versus salt density ρ_b for various membrane permittivities. The characteristic curves split the regions associated with repulsive membranes (above the curves) and attractive membranes (below the curves). The remaining model parameters are the same as in Fig. 2.

permittivity value $\varepsilon_m = 60$, the polymer grand potential is positive at biological salt concentrations but negative for dilute electrolytes. Finally, at the value $\varepsilon_m = 107$ (and for larger permittivities), because image interactions switch from repulsive to attractive, i.e., $F(\gamma) \leq 0$ (see also Fig. 3), the membrane becomes purely attractive at all salt densities.

For translocation experiments carried out with different membrane types, it is interesting to characterize the physical regime where the energy barrier at the membrane surface vanishes. Setting Eq. (41) to zero, we find that this occurs at the characteristic membrane charge

$$\sigma_s^* = \frac{\kappa\lambda}{8\pi} F(\gamma). \tag{43}$$

We note that Eq. (43) generalizes the limiting law of Eq. (38) to any permittivity value ε_m. Based on Eq. (43), we show in Fig. 10 the phase diagram characterizing the parameter regimes with attractive membranes (area above each curve) and repulsive membranes (area below each curve). In this figure, the switching of the membrane charge to negative from up to bottom stems from the fact that the attractive image forces for $\varepsilon_m > 107$ have to be compensated by the repulsion between the negative membrane charge and the negative polymer charge in order for the net surface grand potential to cancel out.

The phase diagram in Fig. 10 indicates that at constant membrane permittivity, the larger the electrolyte density, the larger the characteristic membrane charge where the electrostatic grand potential on the surface vanishes. Indeed, we have shown above that the attractive force induced by the surface charge is more susceptible to salt screening than image forces (see, e.g., Fig. 8(b)). Thus, a stronger salt density has to be compensated by a stronger membrane charge to cancel out the net free at the membrane surface. Furthermore, at constant salt concentration, the larger the dielectric discontinuity, the stronger the surface charge. In translocation experiments, the complex picture of this phase diagram can be at least qualitatively checked by observing the approach of a DNA molecule towards membranes with different chemical surface properties.

III. SUMMARY AND CONCLUSIONS

In this work, we have developed an analytical theory accounting for electrostatic membrane-polymer interactions during the approach phase of DNA translocation events. The corresponding DH theory goes beyond the mean field approximation as it includes correlation effects such as image-charge interactions resulting from the dielectric mismatch between the membrane and the surrounding solvent. Within this theory, we have characterized the complex interplay between the polyelectrolyte length, the salt density, the membrane dielectric permittivity, and the membrane charge and size.

In the first part, we considered neutral membranes. We found that in the case of thick membranes, whose permittivity strongly differs from the solvent permittivity, the approach of a long DNA molecule to the membrane costs the electrostatic grand potential of magnitude $|\Delta\Omega_{\rm pol}(0)| = k_BT\ell_B\lambda^2/(2\kappa)$, where λ is the linear DNA charge density. For neutral carbon-based membranes with low dielectric permittivity ($\varepsilon_m \approx 2$), this corresponds to a high energy barrier between 10 k_BT to 100 k_BT depending on the salt concentration. Interestingly, the theory predicts that in the opposite case of engineered membranes with high permittivity $\varepsilon_m \gg \varepsilon_w$,[17,18] the membrane surface becomes an attraction point. More precisely, within the physiological salt density regime, the approach of the polymer to the membrane reduces its grand potential by 10–100 k_BT. We also found that in pure solvents, the electrostatic grand potential becomes independent of the polymer length if the latter exceeds the membrane thickness, i.e., $L \geq d$. In electrolytes, finite size effects related to the polyelectrolyte length die out if the polymer length is larger than the DH screening length, that is, $L \geq \kappa^{-1}$. Most importantly, we showed that for the thinnest graphene-based membranes of thickness $d \approx 6$ Å,[21] the grand potential barrier encountered by the DNA is close to 100 k_BT. This indicates that surface polarization effects studied herein are crucial even for subnanometer membrane sizes.

In the second part, we took into account the finite charge distribution on the membrane surface. We found that even for weakly charged low permittivity membranes, the electrostatic grand potential acquires an attractive branch far enough from the interface and turns to repulsive very close to the membrane. Because the membrane charge attraction is more sensitive to salt screening than repulsive image forces, the increase of the salt concentration makes the membrane less attractive. Furthermore, due to the competition between membrane charge and image charge effects, the sign of the polymer grand potential may depend on the polymer length. We showed that for specific values of the membrane charge and ion density, the membrane will repel short polymers ($L \ll \kappa^{-1}$) but attract long polymers ($L \gg \kappa^{-1}$). We also showed that the same competition may cancel the net electrostatic grand potential on the membrane surface, which we characterized in the phase diagram of Fig. 10 in terms of the salt density, and the membrane charge and permittivity. This phase diagram

and our general conclusions can be tested in translocation experiments.

Finally, we would like to point out limitations in the present modeling. In our first attempt to model electrostatic polymer-membrane interactions, we opted for an evaluation of the polymer's grand potential at the DH level. Our choice is motivated by the analytical transparency of the DH theory. It should be of course emphasized that our quadratic DH level theory neglects non-linear electrostatic interactions. In dilute solutions with bulk density $\rho_b \lesssim 0.01$M, the DH approximation is known to overestimate the electrostatic potential induced by charged sources. Hence, at low electrolyte concentrations, our grand potential curves may overestimate the actual electrostatic energy barrier values. This limitation can be overcome in a future work by including the non-linearity of the electrostatic potential thorough a charge renormalisation procedure[20] or a one-loop evaluation of the grand potential.[24] However, it should be noted that such improvements will involve considerable complexity and mask the transparency of the present theory. Furthermore, the rigid polymer model neglects the entropic fluctuations of the DNA molecule. The double-stranded DNA molecule has a persistence length of about 50 nm, and in the case of low permittivity membranes image charge interactions are expected to greatly enhance it. This justifies our rigid polymer approximation in the most relevant case of carbon-based membranes. The importance of the role played by polymer fluctuations on DNA-membrane interactions can be evaluated in a future work by considering the polymer entropy through a coupling of the Coulomb liquid model with the beyond-MF formulation of the Flory theory.[9] We also note that in the present work, we focused exclusively on the approach phase of translocation events. In the future we would like to extend our theory to the translocation phase, consider dynamical issues, and include hydrodynamic transport. We emphasize that despite the limitations of the present theory, our main conclusions can be tested in translocation experiments and the theory can hopefully present itself as a starting point for more sophisticated models. The mapping between the membrane dielectric properties and the polymer grand potential that we identified in this work may also allow to improve our control over DNA-membrane interactions via the chemical engineering of membrane materials.

ACKNOWLEDGMENTS

This work has been supported in part by Aalto University's Energy Efficiency project EXPECTS. T.A.-N. has also been supported by the Academy of Finland through its COMP Center of Excellence Grant No. 284621.

APPENDIX A: DEBYE-HÜCKEL LEVEL GRAND POTENTIAL

We present here the DH expansion of the grand potential of the electrolyte. The theory is formulated for general charge distributions in Ref. 23 and thus we will present only the general lines of the derivation. The grand canonical partition function of the charged liquid is given by the functional integral[23]

$$Z_G = \int \mathcal{D}\phi\, e^{-H[\phi]}, \tag{A1}$$

with the Hamiltonian functional

$$H[\phi] = \int d\mathbf{r} \left[\frac{\epsilon(\mathbf{r})}{2\beta e^2} [\nabla\phi(\mathbf{r})]^2 - i\sigma(\mathbf{r})\phi(\mathbf{r}) - \sum_i \lambda_i\, e^{iq_i\phi(\mathbf{r})} \right], \tag{A2}$$

where $\mathbf{r}$ stands for the position vector, $\beta = 1/(k_B T)$ is the inverse temperature, e the electron charge, and $\epsilon(\mathbf{r})$ the dielectric permittivity function. Moreover, the function $\sigma(\mathbf{r})$ accounts for immobile charge distributions in the system. The summation in the third term of Eq. (A2) runs over the ionic species of the electrolyte, each with fugacity λ_i and valency q_i. Finally, within the same field-theoretic representation, local ion densities are given by

$$\rho_i(\mathbf{r}) = \lambda_i \left\langle e^{iq_i\phi(\mathbf{r})} \right\rangle_\phi, \tag{A3}$$

where the bracket $\langle\cdot\rangle_\phi$ denotes the average over fluctuating potential configurations taken with respect to the functional (A2).

The DH approximation consists in Taylor expanding the functional (A2) at the quadratic order in the fluctuating potential $\phi(\mathbf{r})$. One gets the DH functional in the form

$$H_0[\phi] = \int d\mathbf{r} \left[\frac{\epsilon(\mathbf{r})}{2\beta e^2} [\nabla\phi(\mathbf{r})]^2 - i\sigma(\mathbf{r})\phi(\mathbf{r}) \right] - V \sum_i \lambda_i + \sum_i \lambda_i \int d\mathbf{r} \left[-iq_i\phi(\mathbf{r}) + \frac{q_i^2}{2}\phi^2(\mathbf{r}) \right]. \tag{A4}$$

As discussed in the Conclusion, the above approximation is valid at large monovalent salt densities. In dilute salt where the electrostatic potential becomes large, the Taylor expansion should be performed around the solution of the non-linear PB equation.[24] Evaluating now in the bulk region ion density (A3) within the same DH approximation gives

$$\rho_{i,b} = \lambda_i \left[1 + iq_i \langle\phi(\mathbf{r})\rangle_\phi - \frac{q_i^2}{2} \left\langle \phi^2(\mathbf{r}) \right\rangle_\phi \right]_b, \tag{A5}$$

where the subscript b means that the field theoretic averages should be evaluated in bulk, i.e., far from any charged macromolecules breaking the spherical symmetry of the electrolyte. Noting that the average electric field should be zero in bulk, i.e., $\langle\phi(\mathbf{r})\rangle_{\phi,b} = 0$, and inverting Eq. (A5) in the DH approximation gives

$$\lambda_i = \rho_{i,b} \left(1 + \frac{q_i^2}{2} v_{\mathrm{DH},b} \right), \tag{A6}$$

where we defined the bulk limit of the DH Green's function $v_{\mathrm{DH},b} = \left\langle \phi^2(\mathbf{r}) \right\rangle$ for $\mathbf{r}$ in the bulk region. By inserting into Eq. (A4) the expression for fugacity (A6) together with the electroneutrality condition $\sum_i \rho_{ib} q_i = 0$, neglecting the terms beyond the one-loop level, and restricting ourselves to the case of a symmetric electrolyte composed of two ionic species with $\rho_{+b} = \rho_{-b} = \rho_b$ and $q_+ = -q_- = q$, the Hamiltonian functional becomes

$$H_0[\phi] = \int \frac{d\mathbf{r}d\mathbf{r}'}{2} \phi(\mathbf{r}) v_{\mathrm{DH}}^{-1}(\mathbf{r},\mathbf{r}')\phi(\mathbf{r}') - i \int d\mathbf{r}\sigma(\mathbf{r})\phi(\mathbf{r}), \tag{A7}$$

where we defined the DH kernel as

$$v_{\rm DH}^{-1}(\mathbf{r},\mathbf{r}') = \left[-\frac{1}{\beta e^2}\nabla\cdot\varepsilon(\mathbf{r})\nabla + 2\rho_b q^2\right]\delta(\mathbf{r}-\mathbf{r}'). \quad \text{(A8)}$$

We note that deriving Eq. (A8), we dropped the constant term $V\sum_i \lambda_i$ in Eq. (A4) and the term linear in the potential $\phi(\mathbf{r})$ disappeared due to the electroneutrality condition. Computing the DH-level partition function with Eqs. (A1) and (A7) gives

$$Z_0 = \det{}^{1/2}(v_{\rm DH})\exp\left[-\int\frac{\mathbf{dr}d\mathbf{r}'}{2}\sigma(\mathbf{r})v_{\rm DH}(\mathbf{r},\mathbf{r}')\sigma(\mathbf{r}')\right]. \quad \text{(A9)}$$

From the definition of the grand potential $\Omega_{\rm DH} = -k_BT\ln Z_0$, we finally get the latter as the superposition of the ionic and polymer free energies $\Omega_{\rm DH} = \Omega_{\rm ion} + \Omega_{\rm pol}$, each contribution, respectively, given by $\Omega_{\rm ion} = -k_BT\ln\det{}^{1/2}(v_{\rm DH})$ and

$$\Omega_{\rm pol} = k_BT\int\frac{\mathbf{dr}d\mathbf{r}'}{2}\sigma(\mathbf{r})v_{\rm DH}(\mathbf{r},\mathbf{r}')\sigma(\mathbf{r}'). \quad \text{(A10)}$$

APPENDIX B: ELECTROSTATIC GREEN'S FUNCTION IN SLIT GEOMETRY

In this Appendix, we explain the general lines of the inversion of DH kernel equation (A8) in the planar membrane geometry depicted in Fig. 1. Due to the plane geometry where the Green's function satisfies translational symmetry along the x and the y axes, i.e., $v_{\rm DH}(\mathbf{r},\mathbf{r}') = v_{\rm DH}(z,z',\mathbf{r}_\parallel-\mathbf{r}'_\parallel)$, we can Fourier-expand the Green's function as

$$v_{\rm DH}(\mathbf{r},\mathbf{r}') = \int\frac{d^2\mathbf{k}}{4\pi^2}\,e^{i\mathbf{k}\cdot\left(\mathbf{r}_\parallel-\mathbf{r}'_\parallel\right)}\tilde{v}_{\rm DH}(z,z'). \quad \text{(B1)}$$

In Eq. (B1), the dependence of the Fourier expanded Green's function on the wave vector $\mathbf{k}$ is implicit. Moreover, the dielectric permittivity profile reads

$$\varepsilon(z) = \varepsilon_w\theta(-z) + \varepsilon_m\theta(z)\theta(d-z) + \varepsilon_w\theta(z-d), \quad \text{(B2)}$$

where $\theta(z)$ is the Heaviside step function. By inserting the expansion (B1) into the kernel equation (A8), the latter simplifies as

$$\left[\partial_z\varepsilon(z)\partial_z - p^2\right]\tilde{v}_{\rm DH}(z,z') = -\frac{e^2}{k_BT}\delta(z-z'), \quad \text{(B3)}$$

with $p = \sqrt{k^2+\kappa^2}$ and the DH screening parameter $\kappa = 8\pi q^2\ell_B\rho_b$. For the source charge located on the right side of the membrane $z' > d$, the piecewise homogeneous solution is

$$\begin{aligned}\tilde{v}_{\rm DH}(z,z') = {}& C_1e^{pz}\theta(-z) + \left[C_2e^{kz} + C_3e^{-kz}\right]\theta(z)\theta(d-z)\\ &+ \left[C_4e^{pz} + C_5e^{-pz}\right]\theta(z-d)\theta(z'-z)\\ &+ C_6e^{-pz}\theta(z-z'). \end{aligned} \quad \text{(B4)}$$

For the source located in the left half-space $z' < 0$, the solution is given by

$$\begin{aligned}\tilde{v}_{\rm DH}(z,z') = {}& C_1e^{pz}\theta(z'-z)\\ &+ \left[C_2e^{pz} + C_3e^{-pz}\right]\theta(-z)\theta(z-z')\\ &+ \left[C_4e^{kz} + C_5e^{-kz}\right]\theta(z)\theta(d-z)\\ &+ C_6e^{-pz}\theta(z-d). \end{aligned} \quad \text{(B5)}$$

The integration constants C_i with $1\le i\le 6$ are to be determined by applying in each case the continuity of the Green's function $\tilde{v}_{\rm DH}(z,z')$ and the displacement field $\varepsilon(z)\partial_z\tilde{v}_{\rm DH}(z,z')$ at the boundaries $z=0$, $z=d$, and at $z=z'$. After somewhat tedious algebra we get

$$\tilde{v}_{\rm DH}(z\le 0, z'\le 0) = \tilde{v}_b(z-z') + \frac{2\pi\ell_B}{p}\frac{\Delta\left(1-e^{-2kd}\right)}{1-\Delta^2e^{-2kd}}e^{p(z+z')}, \quad \text{(B6)}$$

$$\tilde{v}_{\rm DH}(z\ge d, z'\ge d) = \tilde{v}_b(z-z') + \frac{2\pi\ell_B}{p}\frac{\Delta\left(1-e^{-2kd}\right)}{1-\Delta^2e^{-2kd}}e^{p(2d-z-z')}, \quad \text{(B7)}$$

and

$$\tilde{v}_{\rm DH}(z,z') = \tilde{v}_b(z-z') + \frac{2\pi\ell_B}{p}\times\frac{(1-\Delta^2)e^{(p-k)d} + \Delta^2e^{-2kd} - 1}{1-\Delta^2e^{-2kd}}e^{-p|z-z'|}, \quad \text{(B8)}$$

for $z'\le 0$ and $z\ge d$, or $z'\ge d$ and $z\le 0$. In Eqs. (B6)-(B8), the dielectric discontinuity function is defined as

$$\Delta = \frac{\varepsilon_w p - \varepsilon_m k}{\varepsilon_w p + \varepsilon_m k}. \quad \text{(B9)}$$

We finally note that in Eqs. (B6)–(B8), we introduced the bulk part of the Fourier transformed DH Green's function

$$\tilde{v}_b(z-z') = \frac{2\pi\ell_B}{p}e^{-p|z-z'|}. \quad \text{(B10)}$$

[1]M. Hi, *The Cell Cycle: Principles of Control* (New Science Press, London, 2007).
[2]B. Alberts, *Molecular Biology of the Cell* (Garland Science, New York, 2002).
[3]N. X. Wang and H. A. von Recum, Macromol. Biosci. **11**, 321 (2011).
[4]D. H. Kaye, *The Double Helix and the Law of Evidence* (Harvard University Press, Massachusetts, 2010).
[5]S. F. Edwards, Proc. Phys. Soc. **85**, 613 (1965).
[6]R. Podgornik and B. Zeks, J. Chem. Soc., Faraday Trans. 2 **84**, 611 (1988).
[7]R. Podgornik, Chem. Phys. Lett. **174**, 191 (1990).
[8]R. Podgornik, J. Phys. Chem. **95**, 5249 (1991).
[9]S. Tsonchev, R. D. Coalson, and A. Duncan, Phys. Rev. E **60**, 4257 (1999).
[10]H. Seki, Y. Y. Suzuki, and H. Orland, J. Phys. Soc. Jpn. **76**, 104601 (2007).
[11]R. Kumar and M. Muthukumar, J. Chem. Phys. **131**, 194903 (2009).
[12]S. Buyukdagli and T. Ala-Nissila, Langmuir **30**, 12907 (2014).
[13]S. Qiu, Y. Wang, B. Cao, Z. Guo, Y. Chen, and G. Yang, Soft Matter **11**, 4999 (2015).
[14]S. Buyukdagli, R. Blossey, and T. Ala-Nissila, Phys. Rev. Lett. **114**, 088303 (2015).
[15]C.-H. Cheng and P.-Y. Lai, Phys. Rev. E **70**, 061805 (2004).
[16]A. G. Cherstvy and R. G. Winkler, J. Phys. Chem. B **116**, 9838 (2012).
[17]Z. M. Dang, L. Wang, Y. Yin, Q. Zhang, and Q. Q. Lei, Adv. Mater. **19**, 852 (2007).
[18]A. Dimiev, D. Zakhidov, B. Genorio, K. Oladimeji, B. Crowgey, L. Kempel, E. J. Rothwell, and J. M. Tour, Appl. Mater. Interfaces **5**, 567 (2013).
[19]M. Abramowitz and I. A. Stegun, *Handbook of Mathematical Functions* (Dover Publications, New York, 1972).
[20]S. Buyukdagli, M. Manghi, and J. Palmeri, Phys. Rev. E **81**, 041601 (2010).
[21]S. Garaj, W. Hubbard, A. Reina, J. Kong, D. Branton, and J. A. Golovchenko, Nature **467**, 190 (2010).
[22]H. Chang, F. Kosari, G. Andreadakis, M. A. Alam, G. Vasmatzis, and R. Bashir, Nano Lett. **4**, 1551 (2004).
[23]R. R. Netz, Eur. Phys. J. E **5**, 189 (2001).
[24]S. Buyukdagli, C. V. Achim, and T. Ala-Nissila, J. Chem. Phys. **137**, 104902 (2012).